ORIGINAL ARTICLE

Nano-silica and SiO$_2$/CaCO$_3$ nanocomposite prepared from semi-burned rice straw ash as modified papermaking fillers

Fatma A. Morsy [a,*], **Said M. El-Sheikh** [b], **Ahmed Barhoum** [c]

[a] *Paper and Printing Lab., Chemistry Department, Faculty of Science, Helwan University, Cairo, Egypt*
[b] *Nanostructure Materials Division, Advanced Materials Department, Central Metallurgical Research & Development Institute (CMRDI), P.O. Box 87, Helwan 11421, Cairo, Egypt*
[c] *Department of Materials and Chemistry, Vrije Universiteit Brussel, Pleinlaan 2, 1050 Brussels, Belgium*

Abstract Silica (SiO$_2$) nanoparticles and silica/calcium carbonate (SiO$_2$/CaCO$_3$) core–shell nanocomposites were prepared by sol–gel technique as fillers for papermaking application. Semi-burned rice straw ash (SBRSA), as waste material, was used to prepare the targeted fillers. Preparation of SiO$_2$ nanoparticles and SiO$_2$/CaCO$_3$ nanocomposites was carried out using Na$_2$SiO$_3$ solution that was prepared from SBRSA and CaCO$_3$ nanoparticles of 30–70 nm. The targeted SiO$_2$/CaCO$_3$ nanocomposites were prepared with different molar ratio of SiO$_2$:CaCO$_3$ 1:15, 1:10 and 1:5. The percentage of silica increased from 62.5% to 82.9% by thermal treatment of SBRSA at 800 °C for 2 h. The prepared SiO$_2$ nanoparticles and SiO$_2$/CaCO$_3$ nanocomposites were characterized by using XRD, XRF, TEM, FT-IR and Zeta potential. The results indicate that a pure semi-crystalline SiO$_2$ nanoparticle and semi-crystalline shell of SiO$_2$ coated CaCO$_3$ core particles were produced. The work extended also to investigate the effect of the prepared fillers on physical, mechanical and optical properties of paper.

Application of the prepared SiO$_2$ nanoparticles and SiO$_2$/CaCO$_3$ nanocomposites improved the optical properties of paper (brightness, whiteness and opacity) but it slightly reduced the mechanical properties when compared to commercial precipitated CaCO$_3$ (PCC) filler.

The results showed that the retention of SiO$_2$ nano-particles was highly increased. The retention of the prepared nanocomposites increased along with increasing of SiO$_2$:CaCO$_3$ molar ratio.

* Corresponding author. Tel.: +20 01019830883; fax: +20 2 25552468.
E-mail address: fatma_a_morsy@yahoo.com (F.A. Morsy).
Peer review under responsibility of King Saud University.

1. Introduction

In paper industry, finely-divided white mineral fillers are added to increase the paper brightness, opacity and improve the paper's quality while having reduced costs by replacing the fibre (Gupta, 2007). The filler particles serve to fill the spaces

and crevices between the fibres; thus improving the properties of the sheet. The common papermaking fillers are clay (kaolin), calcium carbonate, talc (magnesium silicate) and titanium oxide (Smook, 1997).

Modification of calcium carbonate filler with silica-containing substances has been proposed to obtain modified filler suspension with high degree of stability and acid-resistant properties (Snowden et al., 2000; Kim and Lee, 2002; Shen et al., 2008, 2010). Various surface coating approaches have been introduced to improve the light scattering of pigments. The light scattering from calcium carbonate particles can be increased by coating the granules with a thin continuous layer of higher refractive index material (Lattaud et al., 2006).

Silica has good properties such as a high specific surface area, high gas absorbability and high oil absorption. These properties are added to the coated pigment specifications (Park et al., 2007). It is also one of the most effective chemicals for paper coating due to its high brightness, opacity, porosity, hydrophilicity. The application of these materials, for instance, as fillers in the paper industry may contribute to the fibre-to-fibre bonding, when coated with silica thus improving paper strength (Gamelas et al., 2011; Lourenço et al., 2013). Silica is introduced as nano-particles with core–shell structure representing a new type of constructional units; such materials enhance physical and chemical properties, thus allowing a broader range of applications compared to the single components (Hall et al., 2000; Vestal and Zhang, 2002; Bala et al., 2007).

The objective of this work is to prepare fillers in a nano- size from waste material to reduce disposal and pollution problems in addition to improving paper filler performance. Also to avoid the reverse effect of filler in reducing the paper strength. The main goal is to prepare (a) nano-silica from the semi-burned rice straw ash (b) silica/calcium carbonate nanocomposite. The prepared fillers were characterized, and therefore the effect on handsheet properties was investigated.

2. Experimental

2.1. Materials

A semi-burned rice straw ash (SBRSA) was obtained from gas production unit of rice straw located at El-Azazy village, Zagazig, Egypt. An analytical grade calcium oxide (CaO, 97% on a dry basis, Acros Organics) and pure CO_2 gas (99.8% supplied by Industrial Gases Company, El-Hawamdia, Giza, Egypt) were used in the preparation of $CaCO_3$ nano-particles. Bleached kraft hardwood and softwood pulps, polyacrylamide suspension (47% solid content) as a retention aid, commercial PCC (1.5 μm length and 250–300 nm in diameter) as reference filler for comparison (supplied by Rakta Company, Alexandria, Egypt) were used for paper handsheet preparation.

2.2. Filler preparation

2.2.1. Preparation of sodium silicate and silica nano-particles
A SBRSA sample was burned at 800 °C for 2 h to remove all the residual hydrocarbons. The produced powder was then sieved. Fraction size less than 0.71 mm (about 54.77%) was selected to perform the experiments. Concentrated sodium silicate Na_2SiO_3 solution was obtained from SRBRA by using alkali leaching process. All the leaching experiments were carried out in covered Teflon beaker (250 ml). Each experiment was performed by dissolving a calculated amount of NaOH in distilled water and then 10 gm of SBRSA was added gradually to attain stoichiometry (NaOH:SiO_2) 3:1 and liquid/solid ratio 10/1. The mixture was heated at 100 °C for 4 h under vigorous constant stirring. After the reaction time completed, the slurry was filtered then washed with distilled water. The concentration of the silica in the obtained solution was measured by ICP and the result showed that the dissolved silica equals 0.735 M with 94.5% extraction efficiency. Silica nanoparticles were obtained by adding gradually 12 wt.% H_2SO_4 solution to the prepared Na_2SiO_3 solution with constant stirring until a pH 10 is reached. The formed silica gel was aged for 24 h and then it was disintegrated, washed with water and ethanol then dried at 120 °C in a drying oven for at least 24 h to produce silica xerogel. The dried xerogel was washed with distilled water to make sure it is free of Na_2SO_4 and calcinated at 300 °C to produce SiO_2 nano-particles (Zaky et al., 2008).

2.2.2. Preparation of nano-calcium carbonate
$CaCO_3$ nano-particles were prepared by using the reaction system $Ca(OH)_2$–H_2O–CO_2 as described in our previous work (El-Sheikh et al., 2013; Barhoum et al., 2014). Bulk CaO was firstly calcined at 1000 °C for 2 h then slaked into lime milk in mono-distilled water at 80 °C. The lime milk was cooled to room temperature (20 °C). At this temperature, the CO_2 gas was injected into the lime milk (1000 mL min^{-1} flow rate and 1 M CaO concentration) with vigorous stirring. The pH value and electric conductivity of the reaction solution were recorded on-line with a pH-meter (Jenway 3305) and a conductometer (Jenway 4510). When the pH value decreased from 14 to 9 and the electric conductivity showed a sharp decrease, this was an indication that the reaction was completed, the CO_2 flow was stopped. $CaCO_3$ particles were obtained and dried at 120 °C in a drying oven for at least 24 h.

2.2.3. Preparation of silica/calcium carbonate nanocomposite
SiO_2/$CaCO_3$ nanocomposites were prepared via a step-by-step method to produce a core–shell structure (Bala et al., 2007). The core $CaCO_3$ nano-particles were obtained in the first step of a carbonation method and SiO_2 layer was coated on the core in the second step of sol-precipitation method from precursor of Na_2SiO_3·9H_2O (Gamelas et al., 2011). The prepared $CaCO_3$ nano-particles were dispersed in 150 mL distilled water using high shear mixer of 3000 rpm for 30 min. The prepared slurry was exposed to high ultrasound waves using the W-385 Sonicator for 30 min. to completely break the agglomerates. The prepared Na_2SiO_3 solution was gradually added to the suspension. The molar ratio of SiO_2/$CaCO_3$ nanocomposites was designed and controlled to be 1:15, 1:10 and 1:5 of the samples CS1, CS2 and CS3, respectively. The mixture was heated up to 80 °C with vigorous constant stirring. The pH value was adjusted to 9 by gradual addition of 6 wt.% H_2SO_4 solution for one hour. Then the mixture was aged for 3 h. The produced slurry was cooled, filtered and rinsed with distilled water to be sure it is free of Na_2SO_4. The SiO_2/$CaCO_3$ nanocomposite powder dried at 120 °C for 24 h then at 300 °C for 3 h.

2.3. Handsheet preparation

Handsheets of paper were prepared with target basis weight of 60 g/m^2 according to TAPPI Standard T-205. The fibre employed in this study was a mixed chemical wood pulp with a hardwood/softwood ratio of 85:15 (wt.%). The prepared fillers (silica nano-particles and $SiO_2/CaCO_3$ nanocomposites) were added to the prepared pulp stock at 15% on dry pulp. Unloaded and commercial PCC loaded handsheets (reference handsheets) were also prepared for comparison. In advance, cationic polyacrylamide was added with a concentration of about 0.1% to dry pulp basis to increase the fillers' retention.

2.4. Characterization of the prepared nano-fillers

The produced nano-fillers were characterized by different techniques as follows:

X-ray diffractometer (XRD, Bruker AXS D8, Germany), with Cu Kα (λ = 1.5406 Å) radiation and a secondary monochromator, was used to preform the phase identification of the prepared silica, $CaCO_3$ nano-particles and $SiO_2/CaCO_3$ nanocomposites. X-ray fluorescence (XRF) Axios, Sequential WD-XRF, PANalytical 2005 (Netherlands) was used to determine the metallic ion impurities in SBRSA and the produced silica. Scanning Electron Microscope (SEM, JEOL instrument model JSM-5410) was used to characterize the microstructure of the obtained fillers. Transmission electron microscopy (TEM, JEOL-JEM-1230, Tokyo, Japan) was used to investigate the morphology information of the samples such as particle size and particle shape. Fourier Transform Infrared (FT-IR) spectra (Jasco FT-IR-3600 plus Japan) was used to detect the existence of organic compounds and lattice water incorporating of excess hydroxide species in the sample. Zeta potentials of suspension samples were measured at room temperature using a Zeta meter 3.0 equipped with a microprocessor unit (Malvern Instrument Zeta Sizer 2000). Laser ablation inductively coupled plasma-mass spectrometry (LA-ICP-MS) determined the concentration of the prepared Na_2SiO_3 solution. The analyses were carried out at FM involving a Varian ICP-MS and a New Wave UP213 laser, for direct introduction of solid samples.

2.5. Characterization of the prepared handsheets

The properties of paper handsheets were evaluated using standard testing for physical, mechanical and optical properties. The ash content was conducted in a muffle furnace at 525 °C

Table 2 XRF analysis of thermally treated SBRSA with fraction size less than 0.71 mm.

Element	Compound formula	Concentration (%)
Na	Na_2O	1.026
Mg	MgO	2.729
Al	Al_2O_3	0.774
Si	SiO_2	82.972
P	P_2O_5	0.267
S	SO_3	0.240
K	K_2O	2.711
Ca	CaO	2.528
Ti	TiO_2	0.130
Mn	MnO	0.317
Fe	Fe_2O_3	1.571
Cu	CuO	0.016
Zn	ZnO	0.018
Sr	SrO	0.023
Pb	PbO	0.007
Cl	Cl	0.171
L.O.I		4.500
Total		100.00

Table 3 XRF analysis of silica nano-particles prepared from SBRSA.

Element	Compound formula	Concentration (%)
Si	SiO_2	99.80
Na	Na_2O	0.110
K	K_2O	0.032
Al	Al_2O_3	0.031
Fe	Fe_2O_3	0.015
Total		100.00

Table 1 XRF analysis for semi-burned rice straw as received.

Element	Compound formula	Concentration (%)
Na	Na_2O	1.38
Mg	MgO	0.14
Al	Al_2O_3	0.33
Si	SiO_2	62.5
P	P_2O_5	0.26
S	SO_3	0.56
K	K_2O	1.98
Ca	CaO	0.91
Ti	TiO_2	0.11
Mn	MnO	0.53
Fe	Fe_2O_3	0.37
Cl	Cl	1.68
L.O.I		29.25
Total		100.00

Table 4 XRF analysis of $SiO_2/CaCO_3$ nanocomposites CS1, CS2 and CS3.

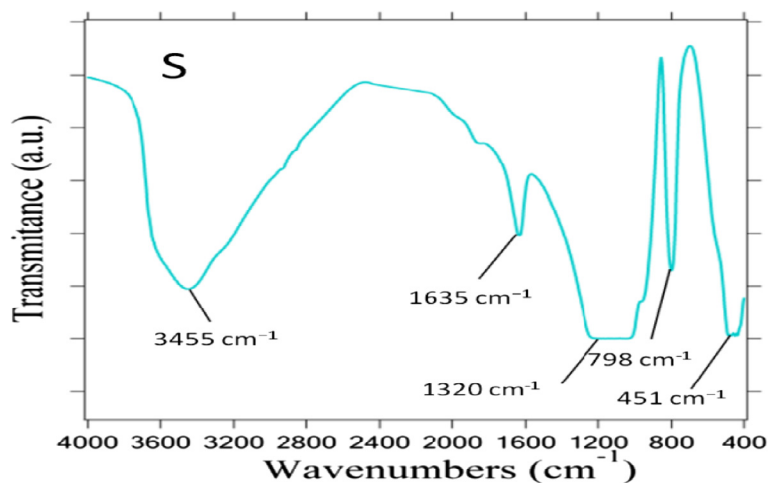| Element	Compound formula	Concentration (%)		
		CS1	CS2	CS3
Na	Na_2O	0.060	0.061	0.060
Mg	MgO	0.188	0.187	0.187
Al	Al_2O_3	0.094	0.094	0.094
Si	SiO_2	1.822	2.123	2.997
P	P_2O_5	0.012	0.010	0.013
S	SO_3	0.077	0.077	0.075
Ca	CaO	54.992	53.822	53.812
Fe	Fe_2O_3	0.247	0.248	0.245
Sr	SrO	0.031	0.032	0.032
Cl	Cl	0.033	0.043	0.042
L.O.I	CO_2	41.894	43.303	42.443
Total		100	100	100

Figure 1 FT-IR spectra of silica nano-particles prepared from thermally treated SBRSA.
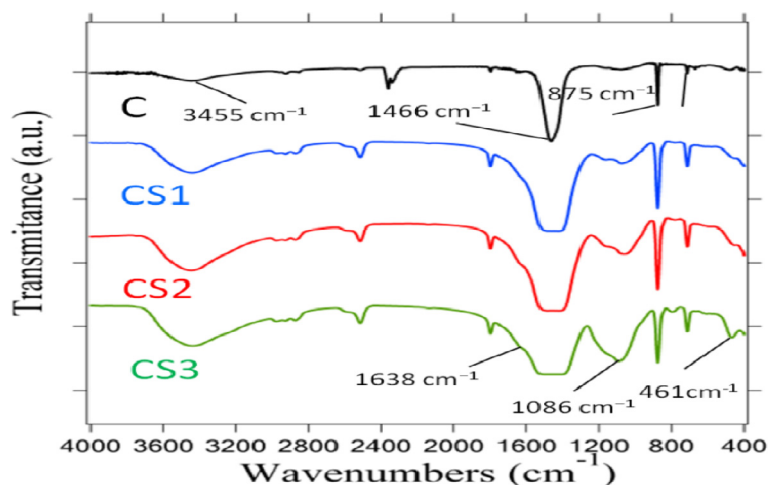

Figure 2 FT-IR spectra of CaCO$_3$ core particles (C) and SiO$_2$/CaCO$_3$ nanocomposites prepared at different SiO$_2$:CaCO$_3$ molar ratios 1:15 (CS1), 1:10 (CS2) and 1:5 (CS3).
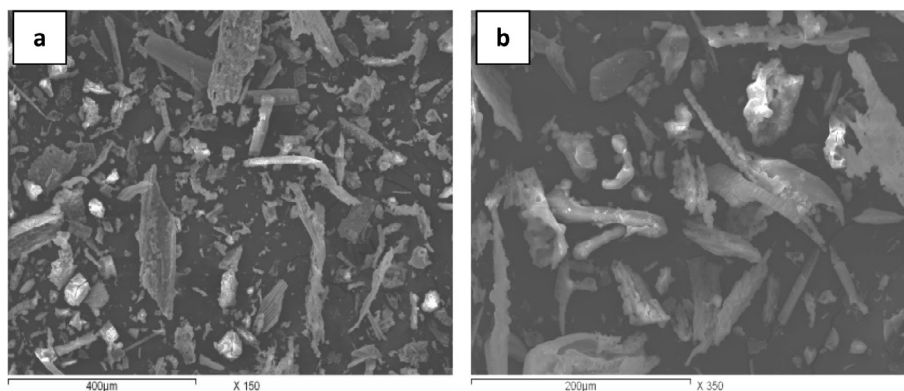

Figure 3 SEM images of thermally treated SBRSA at magnifications (a) 150× and (b) 350×.

according to Tappi test method T211 om-93. The filler retention (R) was calculated as follows:

$$\text{Retention} = \frac{X2 - X0}{X1} \cdot 100\% \qquad (1)$$

Where: X2 = Ash of paper loaded with filler, X0 = Ash of nonloaded paper and X1 = Ash of added filler. The paper grammage in g/m^2 was calculated according to Tappi test method 410.
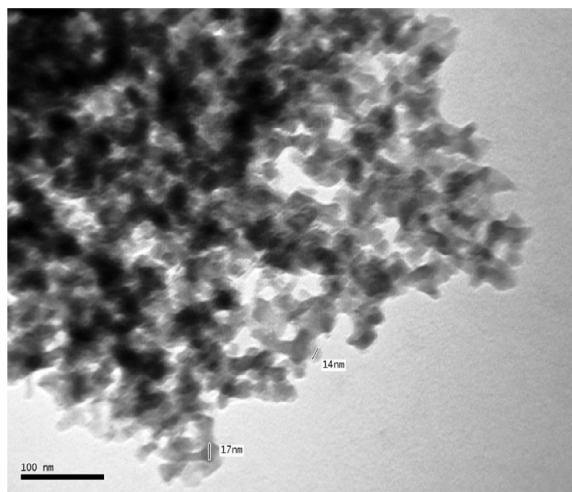
Figure 4 TEM micrograph of silica nano-particles prepared from thermally treated SBRSA.

The thickness was measured based on Tappi 411 using L&W micrometer 51. The density was calculated according to the following equation:

$$d = 1000 \ G/t \qquad (2)$$

where: d = density, kg/m^3, G = grammage, g/m^2, t = thickness, μm.

Bursting was measured using Frank GmbH 1882 burst tester according to Tappi 807. Hounsfield H5KS tensile tester was used to measure tensile strength according to Tappi 404. The internal tearing strength was measured on a pendulum type instrument, A tear tester (L&W 2404) was used according to Tappi 496. All optical tests were qualitative and conducted using integrating reflectometer, model JY9800. The instrument has multifunction; it can be used to measure brightness, whiteness, and opacity. The prepared handsheets' brightness was measured according to ISO 2470:1999. The degree of whiteness was measured according to ISO 11475:1999. The opacity was measured in accordance with ISO 2471:1998.

3. Results and discussion

3.1. XRF chemical analysis

Table 1 shows chemical analysis of SBRSA sample as received by using XRF analysis. The results show that the percentage of SiO$_2$ is 62.5% and the moisture content is 7.4%.

Table 2 represents XRF analysis of thermally treated SBRSA sample. The percentage of silica increased to be 82.9%. The XRF analysis of silica nano-particles indicates that the produced silica has a high purity reaching to 99.8% (Table 3). Table 4 shows that the prepared SiO$_2$/CaCO$_3$ nano-composites (CS1, CS2 and CS3) have SiO$_2$ contents of 1.82%, 2.12% and 2.99%, respectively. It is found that the amount of SiO$_2$ in the produced composites increased with increasing the concentration of SiO$_2$:CaCO$_3$ molar ratio in the coating process.

3.2. FT-IR spectrum

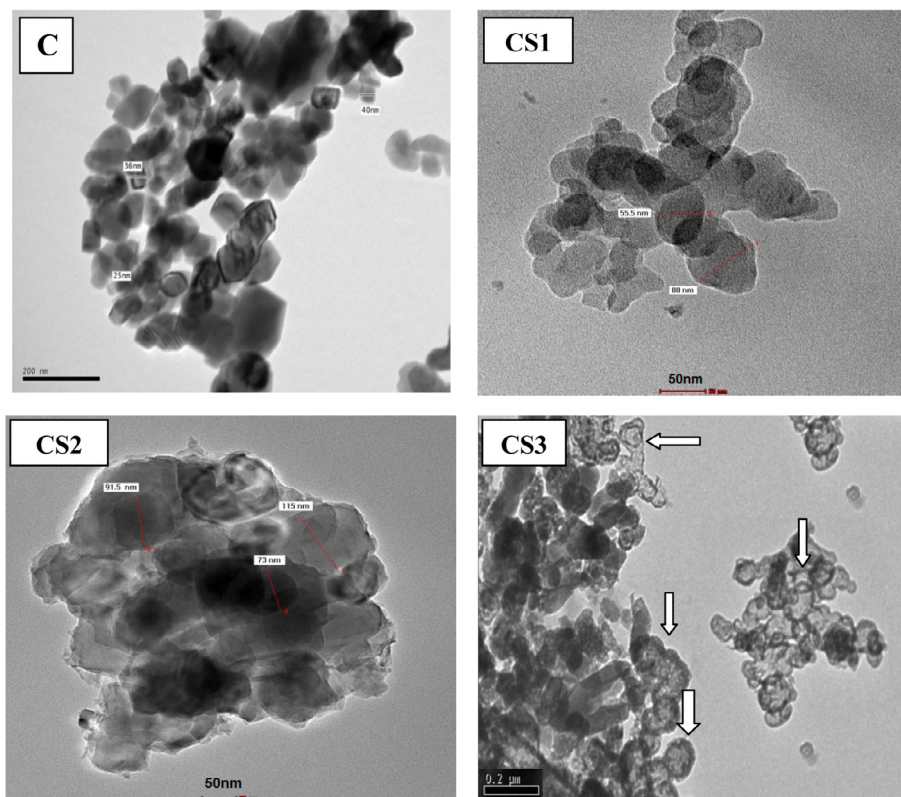The major chemical groups present in silica nano-particles prepared from thermally treated SBRSA are identified by the

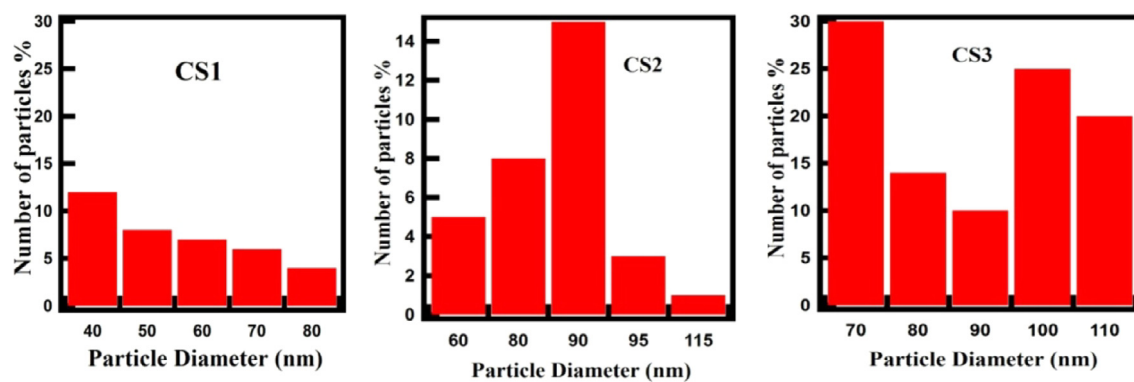**Figure 5** TEM images of CaCO$_3$ core particles (C) and SiO$_2$/CaCO$_3$ nanocomposites (CS1), (CS2) and (CS3).

Figure 6 Particle size distribution of SiO$_2$/CaCO$_3$ nanocomposites (CS1, CS2 and CS3).
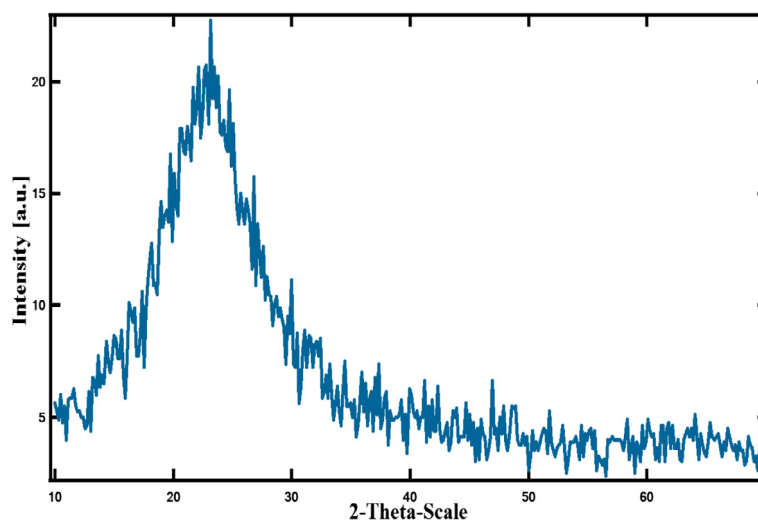

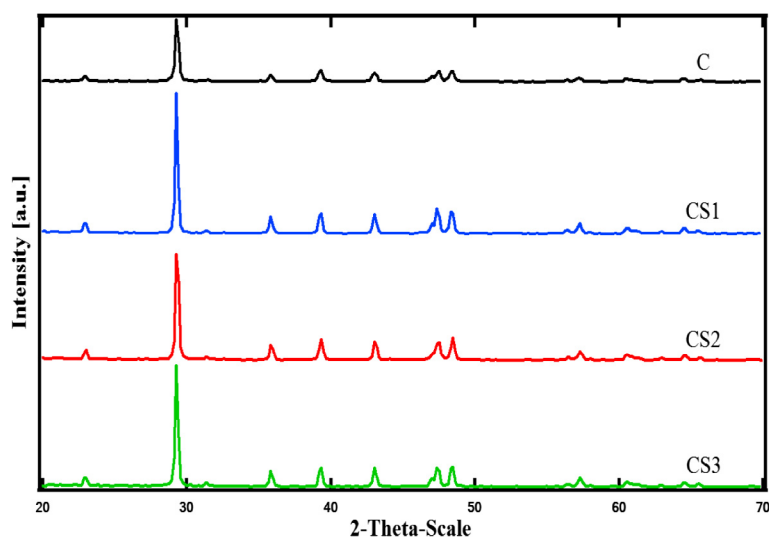**Figure 7** XRD patterns of silica nano-particles prepared from thermally treated SBRSA.

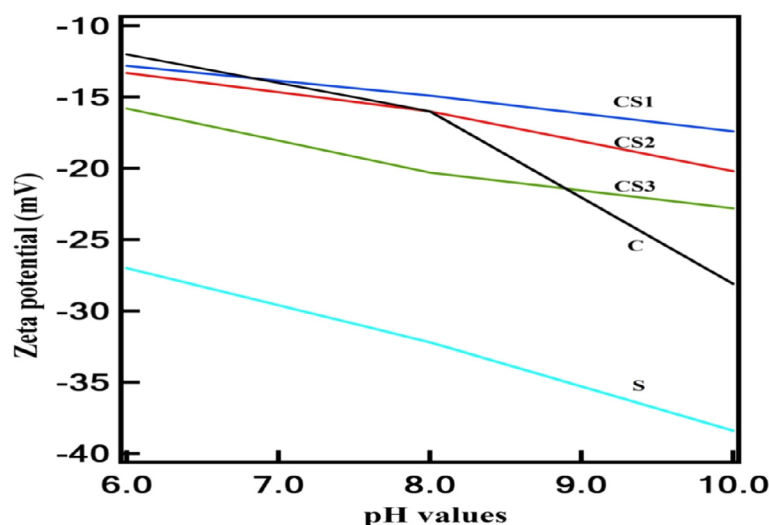**Figure 8** XRD patterns of CaCO$_3$ core particles (C) and SiO$_2$/CaCO$_3$ nanocomposites (CS1, CS2 and CS3).

Figure 9 Zeta Potential versus pH values of $CaCO_3$ core particles (C), silica nano-particles prepared from thermally treated SBRSA and $SiO_2/CaCO_3$ nanocomposites (CS1, CS2 and CS3).

Table 5 Average crystal size, particle size, particle morphology, silica content and surface charge of SiO2/CaCO3 nanocomposites.

Samples		SiO_2: $CaCO_3$ molar ratio	Results				
			Av. crystal size, nm	Particle size range (nm)	Particle morphology	SiO_2 content (%)	Surface charge (mV)
$CaCO_3$ Core	C	–	57.4	30–70	Rhombohedral	0	−17.4
$SiO_2/CaCO_3$	CS1	1:15	92.9	40–80	Rhombohedral	1.82	−20.2
Nano- composite	CS2	1:10	80.3	60–90	Sphere-like	2.12	−22.8
	CS3	1:5	80.2	70–110	Spherical	2.99	−28.1

FT-IR spectra as shown in Fig. 1. The broad absorption band at 3455.8 cm^{-1} and the peak at 1635 cm^{-1} are due to silanol OH groups and adsorbed water, respectively. The predominant absorbance peak at 1320 cm^{-1} is due to siloxane bonds (Si–O–Si). The peaks at 1093, 798.3, and 451.2 cm^{-1} are due to the asymmetric, symmetric and the bending modes of SiO_2, respectively (Kamath and Proctor, 1998).

Fig. 2 shows the FT-IR spectra of the $CaCO_3$ core nano-particles and the $SiO_2/CaCO_3$ nanocomposites CS1, CS2 and CS3 with SiO_2:$CaCO_3$ molar ratios 1:15, 1:10 and 1:5, respectively. There are significant absorption peaks due to CO_3^{-2} group in $CaCO_3$ core particles (C) at 1466.86, 875.13 and 713.66 cm^{-1}, respectively (Nyquist et al., 1997). Because there is no split occurring at the 1465.86 and 875.13 cm^{-1}, one can conclude that the $CaCO_3$ has a calcite structure (standard calcium carbonate infrared spectra). Spectra of $SiO_2/CaCO_3$ nanocomposites CS1, CS2 and CS3 reveal that there are absorption peaks at 3441.8, 1638.87, 1077.01, 797.38 and 463.80 cm^{-1} which confirms the formation of silica (Martinez et al., 1998) besides the absorption peaks of $CaCO_3$, which indicates the presence of both silica and CaCO. The bands at 3441.8 and 1638.87 cm^{-1} are related to the constitutional water and those at 1086.01, 959.72, 797.38 and 461.34 cm^{-1} are attributed to the Si–OH stretching, Si–O–Si asymmetric stretching, symmetric stretching and bending vibrations, respectively.

3.3. Morphology and XRD analysis

Fig. 3 shows the SEM images of thermally treated SBRSA. It is observed that the ash has black with grey particles as a result of different steps of carbon combustion during the rice straw burning. The micrographs show that the SBRSA has mainly needle-like particles.

Fig. 4 shows TEM micrograph of the produced silica. The silica nano-particles have narrow size distribution (particle sizes are ranged from 20–30 nm) with a spherical shape and good dispersion. Fig. 5 shows TEM micrographs of nano-$CaCO_3$ core particles (C) and $SiO_2/CaCO_3$ nanocomposites (CS1, CS2 and CS3). The nano-$CaCO_3$ core particles have rhombohedral structure with particles size range 30–70 nm. $SiO_2/CaCO_3$ nanocomposites CS1, CS2 and CS3 have rhombohedral, sphere-like and spherical morphology, with particle sizes ranging from 40–80, 60–90 and 70–110 nm, respectively. It is noticed that the $SiO_2/CaCO_3$ nanocomposites are brighter than those of the single $CaCO_3$ particles. Fig. 6 represents particle size distribution of $SiO_2/CaCO_3$ nanocomposites (CS1, CS2 and CS3).

Fig. 7 represents X-ray diffraction patterns of silica nano-particles prepared from SBRSA. It is clear that the typical silica is observed at a broad peak centred at $2\theta = 22.5°$, which indicates that the sample is semi-crystalline phase. Fig. 8 shows XRD patterns of the $CaCO_3$ nano-particles and $SiO_2/CaCO_3$

Table 6 Physical, mechanical and optical properties of reference handsheets and handsheets loaded with nano-silica and SiO$_2$/CaCO$_3$ nanocomposite fillers.

Fillers characterization				Handsheet									Retention (%)
				Physical Properties		Mechanical Properties			Optical Properties				
Type of filler	Symbol	Particle size (nm)	Morphology	Grammage g/m^2	Density (kg/m^3)	Burst index (kPa m^2/g)	Tensile index N m/g	Tear index mN m^2/g	Brightness (%)	Whiteness (%)	Opacity (%)		
References	BK	Non	Non	59.5	14.88	4.68	72.74	10.02	72.46	55.5	62.6		Non
	PCC	250 nm 1.5 μm length	Scalenohedral	60.48	14.47	4.17	54.08	9.65	77.97	61.94	76.6		45.5
Silica	S	20–30	Spherical	58.51	7.75	2.94	40.25	11.18	80.47	65.42	78.1		70.8
SiO$_2$/CaCO$_3$ nanocomposite	CS1	40–80	Rhombohedral	61.72	13.74	4.04	54.76	9.68	81.66	68.56	80.2		55.7
	CS2	60–90	Sphere-like	60.17	13.61	3.89	53.17	9.89	81	67.89	81.2		57.5
	CS3	70–110	Spherical	60.24	13.38	3.82	50.44	10.71	81.45	68.19	82.2		60.1

nanocomposites (CS1, CS2 and CS3). The results show that all the diffraction peaks of nano-CaCO$_3$ core particles (C) can be related to a pure calcite phase. The SiO$_2$/CaCO$_3$ nanocomposites CS1, CS2 and CS3 samples have similar diffraction peaks which indicate that the shell layer of SiO$_2$ is semi-crystalline. It can be noticed that the intensities of the peaks at 2-Theta Scale at 23° and 29.5° are increased in the case of CS1, CS2 and CS3 compared to CaCO$_3$ core particles (C). The XRD analysis results are in a good agreement with the results obtained from FT-IR.

3.4. Zeta potential

Fig. 9 shows the result of zeta potential versus pH values (6–10) of the produced silica nano-particles, CaCO$_3$ core particles (C) and SiO$_2$/CaCO$_3$ nanocomposites (CS1, CS2 and CS3). The result shows that the negative surface charges on the produced silica nano-particles increased gradually to more negative values with increasing the pH value (Tsai, 2004). At pH = 10 zeta potential is −38.4 mV. The results show that zeta potential of CaCO$_3$ core nano-particles at pH = 10 is −17.4 mV, while zeta potentials of the prepared composites CS1, CS2 and CS3 are −20.2, −22.8 and −28.1 mV, respectively. It is observed that zeta potential values of the prepared SiO$_2$/CaCO$_3$ nanocomposites are more negative than core particles and these negative values increased gradually with the increase of SiO$_2$:CaCO$_3$ molar ratio.

Table 5 summarizes the obtained results of SiO$_2$/CaCO$_3$ nanocomposites using XRD, TEM, XRF and Zeta potential techniques.

3.5. Properties of handsheets loaded with the prepared nano-fillers

The physical, mechanical and optical properties of reference handsheets (unloaded and commercial PCC loaded handsheets) and handsheets loaded with silica nano-particles (S), and SiO$_2$/CaCO$_3$ nanocomposites (CS1, CS2 and CS3) fillers are summarized in Table 6.

3.5.1. Retention

The results shown in Table 6 reveal that silica nano-particles (S) and SiO$_2$/CaCO$_3$ nanocomposites (CS1, CS2 and CS3) have a higher retention than the commercial PCC; the percentage of increase reaches 34.9% for silica nano-particles, while it varies from 6.1% to 14.4% for SiO$_2$/CaCO$_3$ nanocomposites. The presence of cationic polyacrylamide enhances silica nano-particles and SiO$_2$/CaCO$_3$ nanocomposite aggregation to optimum size. Agglomerated fillers are sufficiently large in size to be retained within the sheet and fill the fibres' gaps. The long-chain cationic polyacrylamide adsorption on the surfaces occurs through either bridging or charge neutralization. Charge neutralization occurs in the vicinity of zero potential (i.e., the isoelectric point) where the aggregation of fine particles (i.e., fines, fillers) is at its maximum point since charge neutralization promotes the bridging through depressing the double layer thickness (Khosravani et al., 2010). Silica nano-particles and SiO$_2$/CaCO$_3$ nanocomposites neutralize the polyelectrolyte charges more aggressively than the other anionic components of pulp stock. Adsorption of silica nano-particles on SiO$_2$/CaCO$_3$ nanocomposite particles screens out repulsive
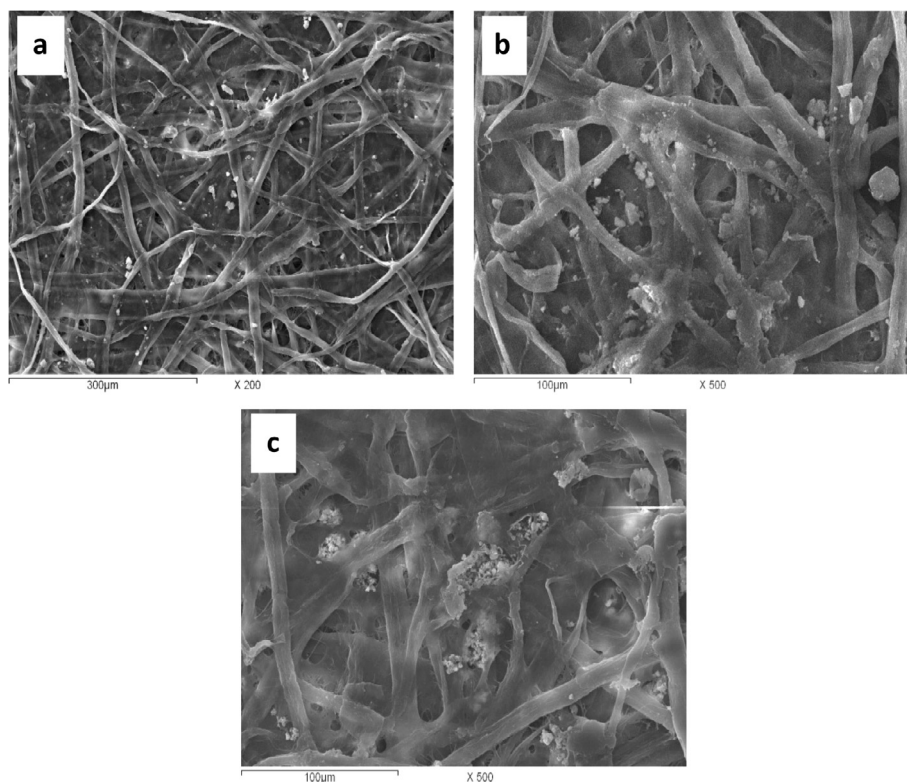
Figure 10 SEM images of handsheets loaded with (a) commercial PCC reference, (b) silica nano-particles and (c) $SiO_2/CaCO_3$ nanocomposite CS1.

electrostatic interactions between the polymers and the surfaces, thus increasing the adsorption and retention. This result is confirmed by the zeta potential measurements, where silica nano-particles have the greatest retention (70.8%) and the highest zeta potential (-38.4 mV). The retention of $SiO_2/CaCO_3$ nanocomposites increased as the surface negativity increased in the order CS1 < CS2 < CS3 as shown in Tables 5 and 6.

3.5.2. Physical properties of handsheets
3.5.2.1. Grammage and handsheet density. Table 6 represents the effect of the prepared silica nano-particles and $SiO_2/CaCO_3$ nanocomposites (CS1, CS2 and CS3) on handsheets' density and grammage at constant pressing action. The results show that silica nano-particles and $SiO_2/CaCO_3$ nanocomposites have lower densities than the unloaded sample (BK) and the PCC loaded handsheets. The percentage of density decrease reached 46.5% for silica nano-particles, while the percentage of decrease varied from 5% to 7.5% for $SiO_2/CaCO_3$ nanocomposites. Silica nano-particles showed the lowest handsheet density and grammage. This may be due to highest retention and smallest particle size of silica nano-particles (20–30 nm) than other ones. The higher retention of silica nano-particles than $SiO_2/CaCO_3$ nanocomposites CS1, CS2 and CS3 led to increasing inter-fibre spacing and reducing handsheet density.

3.5.3. Mechanical properties of handsheets
3.5.3.1. Burst index. Handsheets loaded with silica nano-particles and $SiO_2/CaCO_3$ nanocomposites have lower burst indexes than PCC loaded handsheets as shown in Table 6.

The small particle size of nano-filler led to higher relative amount of fibre surface that can be covered by given mass particles which prevents inter-fibre contact over a larger fraction of the available surface area (Hubbe and Gill, 2004). Silica nano-particles showed the lowest handsheet burst index. This may be due to highest retention and smaller particle size of silica nano-particles than the others. Despite the higher retention value of CS1 than commercial pigment, there is no significant decrease in burst index.

3.5.3.2. Tensile index. The results obtained in Table 6 illustrate that addition of silica nano-particles led to a significant decrease in tensile index. This sample has the highest retention (70.8%). Although nanocomposite samples showed higher retention than PCC, acceptable tensile values were obtained.

3.5.3.3. Tear index. Handsheets loaded with silica nano-particles and $SiO_2/CaCO_3$ nanocomposites (CS1, CS2 and CS3) show higher tear indexes than PCC loaded handsheets (Table 6) the increase reached to 10.9% for CS3 sample. Silica nano-particles show the highest handsheet tear index due to their higher retention and smaller particle size than both $SiO_2/CaCO_3$ nanocomposites and PCC. In addition, the tear indexes of $SiO_2/CaCO_3$ nanocomposites increased with increasing SiO_2 shell thickness.

3.5.4. Optical properties of handsheets
Table 6 illustrates the effect of the prepared nano-fillers on optical properties of the handsheets. Silica nano-particles and $SiO_2/CaCO_3$ nanocomposites significantly improved brightness, whiteness and opacity of the prepared handsheets

compared to unloaded (BK) and commercial PCC loaded handsheets. The reasons for these behaviours are the smaller particle size, larger surface and higher light scattering of silica nano-particles and $SiO_2/CaCO_3$ nanocomposites (CS1, CS2 and CS3) comparing to micron size of PCC (Hubbe and Gill, 2004).The incident light on $SiO_2/CaCO_3$ nanocomposite was refracted on air/silica interface and $SiO_2/CaCO_3$ interface, thus led to imparting $SiO_2/CaCO_3$ nanocomposites higher refractive indices than $CaCO_3$ alone (Bala et al., 2007). $SiO_2/CaCO_3$ nanocomposites increased the optical properties than silica nano-particles. SiO_2 shell thickness has a little effect on brightness and whiteness while it has a significant effect on opacity. In addition, CS3 shows the highest handsheet opacity. The handsheet opacity increased from 4.6% to 7.3% with increasing SiO_2 shell thickness from CS1 to CS3, compared with PCC loaded handsheets. This may be due to high retention of CS3 than CS1 and CS2.

3.5.5. Morphology of handsheets

Figs. 10 shows the surface of handsheets loaded with commercial PCC reference, silica nano-particles (S) and $SiO_2/CaCO_3$ nanocomposite CS1, respectively. Fig. 10a shows bad PCC distribution and more particles were attached on fibre surfaces than on fibre gaps. The high retention of silica nano-particles, high negatively charged surface and the use of high molecular weight polyacrylamide caused aggregation of silica nano-particles as large agglomerates (Fig. 10b). The aggregation of silica nano-particles within paper sheets enhanced optical properties but reduced tensile and burst indexes comparing to commercial PCC as shown in Table 6. Fig. 10c shows that CS1 nanocomposite is uniformly distributed. From the properties of handsheets (Table 6) it was found that the nanocomposite CS1 shows higher mechanical properties than CS2 and CS3. This filler has less negative surface charge and smaller SiO_2 shell thickness than CS2 and CS3. Thus, it may be able to form less aggregate particles to cover more fibre surface and densely fill the fibre gaps.

4. Conclusions

Silica nano-particles and $SiO_2/CaCO_3$ nanocomposite were successfully prepared from sodium silicate solution that was obtained from the semi-burned rice straw ash (SBRSA). The thermal treatment of SBRSA at 800 °C for 2 h concentrated SiO_2 from 60.2% up to 82.9%. XRD patterns showed that the precipitated silica nano-particles have a semi-crystalline phase and Zeta potential −38.4 mV at pH 10. While the negative surface potential of the prepared nanocomposites changed from −20.2, −22.8 to −28.1 mV with increasing $SiO_2:CaCO_3$ molar ratio. TEM images, XRD, FT-IR with zeta potential measurements indicated that the amount of SiO_2 increased with increasing $SiO_2:CaCO_3$ molar ratio at the coating process. The results showed that the retention of silica nano-particles increased due to the high negatively charged surface which caused aggregation in the matrix. Thus, enhanced optical properties but it slightly reduced mechanical properties comparing to commercial PCC. The retention of the prepared $SiO_2/CaCO_3$ nanocomposite also increased with increasing $SiO_2:CaCO_3$ molar ratio. On the other hand, the results revealed that the mechanical properties were not significantly affected while the handsheet brightness, whiteness and opacity were improved compared to commercial PCC.

References

Barhoum, A., Rahier, H., Esmail Abou-Zaied, R., Rehan, M., Dufour, T., Hill, G., Dufresne, A., 2014. Effect of cationic and anionic surfactants on the application of calcium carbonate nanoparticles in paper coating. ACS Appl. Mater. Interfaces. 6, 2734–2744.

Bala, H., Zhang, Y., Ynag, H., Wang, C., Li, M., Lv, X., Wang, Z., 2007. Preparation and characteristics of calcium carbonate/silica nanoparticles with core-shell structure. Colloids Surf., A 294, 8–13.

El-Sheikh, S.M., El-Sherbiny, S., Barhoum, A., Deng, Y., 2013. Effects of cationic surfactant during the precipitation of calcium carbonate nano-particles on their size, morphology, and other characteristics. Colloids Surf., A. 422, 44–49.

Gamelas, J.A.F., Lourenco, A.F., Ferreira, P.J., 2011. New modified filler obtained by silica formed by sol–gel method on calcium carbonate. J. Sol-Gel Sci. Technol. 59 (1), 25–31.

Gupta N., 2007. Effect of various fillers on physical and optical properties of agro-straw papers, A Master Thesis of Science, School of Physics and Material Sciences. Thapar University Patiala, India.

Hall, S.R., Davis, S.A., Mann, S., 2000. Condensation of organosilica hybrid shells on nanoparticle templates: a direct synthetic route to functionalized core-shell colloids. Langmuir 16, 1454–1456.

Hubbe, M.A., Gill, R. A., 2004. Filler particle shape vs. paper properties, A review in 2004 TAPPI Paper Summit - Spring Technical and International Environmental Conference in Atlanta, Georgia, May 2–5, 141–150.

Kamath, S.R., Proctor, A., 1998. Silica gel from rice hull ash: preparation and characterization. Cereal Chem. 75, 484–487.

Khosravani, A., Latibari, A.J., Mirshokraei, S.I., Rahmaninia, M., Nazhad, M.M., 2010. Studying the effect of cationic starch- anionic nanosilica system on retention and drainage. BioResources 5 (2), 939–950.

Kim, D.S., Lee, C.K., 2002. Surface modification of precipitated calcium carbonate using aqueous fluosilicic acid. App. Surf. Sci. 202, 15–20.

Lattaud, K., Vilminot, S., Hirlimann, C., Parant, H., Schoelkopf, J., Gane, P., 2006. Index of refraction enhancement of calcite particles coated with zinc carbonate. Solid State Sci. 8 (10), 1222–1228.

Lourenço, A.F., Gamelas, J.A.F., Zscherneck, C., Ferreira, P.J., 2013. Evaluation of silica-coated PCC as new modified filler for papermaking. Ind. Eng. Chem. Res. 52 (14), 5095–5099.

Martinez, J.R., Ruiz, F., Vorobiev, Y.V., 1998. Infrared spectroscopy analysis of the local atomic structure in silica prepared by sol-gel. J. Chem. Phys. 109 (17), 7511–7514.

Nyquist, R.A., Putzig, C.L., Leugers, M.A., 1997. In: The Handbook of Infrared and Raman Spectra of Inorganic Compounds and Organic Salts, vol. 1. Academic press, San Diego.

Park, J.K., Kim, J.K., Kim, H.K., 2007. TiO₂–SiO₂ composite filler for thin paper. J. Mater. Prod. Technol. 186 (1–3), 367–369.

Shen, J., Song, Z.Q., Qian, X.R., Wang, K.C., Zhang, Y., 2008. Dissolution-inhibiting effect of silicate-based inhibitors on precipitated calcium carbonate filler. China Pulp & Pap. 27 (10), 13–17.

Shen, J., Song, Z., Qian, X., Yang, F., Kong, F., 2010. Nanofillers for papermaking wet end applications. BioResources 5 (3), 1328–1331.

Smook, G.A., 1997. Handbook for Pulp & Paper Technologists, 2nd edition. Angus Wilde Publications Inc., Bellingham, WA.

Snowden, K. J., Wu, K. T., Rodriguez, J. M., 2000. U.S. Patent 6,083,317, Jul. 4.

Tsai, M.S., 2004. The study of formation colloidal silica via sodium silicate. Mater. Sci. Eng., B 106 (1), 52–55.

Vestal, C.R., Zhang, Z.J., 2002. Atom transfer radical polymerization synthesis and magnetic characterization of Mnfe2o4/polystyrene core/shell nanoparticles. J. Am. Chem. Soc. 124 (48), 14312–14313.

Zaky, R., Hessien, M., El-Midany, A., Khedr, M., Abdel-Aal, E., El-Barawy, K., 2008. Preparation of silica nanoparticles from semi-burned rice straw ash. Powder Technol. 185 (1), 31–35.